Absorption coefficient of urban aerosol in Nanjing, west Yangtze River Delta of China

B. L. Zhuang[1, 4, *], T. J. Wang[1, 4], J. Liu[1,2], Y. Ma[3], C. Q. Yin[1], S. Li[1, 4], M. Xie[1, 4], Y. Han[1, 4], J. L. Zhu[1], X. Q. Yang[1, 4], C. B. Fu[1, 4]

[1] School of Atmospheric Sciences, Nanjing University, Xianlin Ave. 163, Nanjing, 210023, China

[2] Department of Geography and Planning, University of Toronto, Toronto, M5S 3G3, Canada

[3] School of Environmental Science and Engineering, Nanjing University of Information Science and Technology, Ningliu Rd. 219, Nanjing, 210044, China

[4] Collaborative Innovation Center of Climate Change, Jiangsu Province, China

[*] Corresponding author, E-mail: blzhuang@nju.edu.cn; Tel.: +862589681156; fax: +862589683797

Abstract: Absorbing aerosols can significantly modulate shortwave solar radiation in the atmosphere, affecting regional and global climate. Aerosol absorption coefficient (AAC) is an indicator to assess the impact of absorbing aerosols on radiative forcing. In this study, the near-surface AAC and absorption angstrom exponent (AAE) in urban Nanjing, China, are characterized on the basis of measurements in 2012 and 2013 using the 7-channel Aethalometer (model AE-31, Magee Scientific, USA). The AAC is estimated with direct and indirect corrections, which result consistent temporal variations and magnitudes of AAC at 532 nm. The mean AAC at 532 nm is about 43.23±28.13 Mm^{-1} in urban Nanjing, which is much lower than that in Pearl River Delta and as the same as that in rural areas (Lin'an) in Yangtze River Delta. The AAC in urban Nanjing shows strong seasonality (diurnal variations), high in cold seasons (at rush hours) and low in summer (in afternoon). It also show synoptic and quasi-two-week cycles in response to weather systems. Its frequency distribution follows a typical lognormal pattern. The 532 nm-AAC ranging from 15 to 65 Mm^{-1} dominates, accounting for more than 72% of the total data samples in the entire study period. Frequent high pollution episodes, such as those

25 observed in June 2012 and in winter 2013, greatly enhanced AAC and altered its temporal variations
26 and frequency distributions. These episodes are mostly due to local emissions and regional pollution.
27 Air masses from northern China to Nanjing can sometimes be highly polluted and lead to high AAC at
28 the site. AAE at 660/470 nm from the Schmid correction (Schmid et al., 2006) is about 1.56, which
29 might be more reasonable than that from the Weingartner correction (Weingartner et al., 2003). Low
30 AAEs mainly appear in summer likely due to high relative humidity (RH) in the season. AAC increases
31 with increasing AAE at a fixed aerosol loading. The RH-AAC relationship is more complex. Overall,
32 AAC peaks around RH values of 40% (1.3<AAE<1.6), 65% (AAE<1.3 and AAE>1.6), and 80%
33 (1.3<AAE<1.6).
34
35 **1 Introduction**
36 Atmospheric aerosols, their loadings having increased in recent years, can significant influence
37 regional or global climate because of their direct and indirect interactions with shortwave solar
38 radiation in the atmosphere (Forster et al., 2007). Absorbing aerosols, which is mostly composed of
39 dust in desert areas and of black carbon (BC) in the regions with frequent human activities, can
40 strongly absorb solar radiation, resulting in changes in the atmospheric circulations and hydrological
41 cycle. Although the warming effect of CO_2 could be greatly offset by the scattering aerosol direct effect
42 in the regions with high aerosol concentrations (Kiehl and Briegleb, 1993), it might be further
43 strengthened by BC aerosols because the warming effect of BC aerosols on the global scale is
44 significant, only surpassed by CO_2 (Jacobson 2002). Menon et al. (2002) suggested that the trend of
45 precipitation in China over the past decades, with increased rainfall in the south and drought in the
46 north, might be related to the variation of BC in the region.

47 Previous studies have focused on the aerosol optical properties, radiative forcing and climate
48 effects in both global and regional scales, using model simulations (Penner et al., 2001; Liao and
49 Seinfeld, 2005; Zhuang et al., 2013a; b) and satellite/ground-based observations (Bellouin et al., 2003;
50 Yan et al., 2008; Wu et al., 2012; Zhuang et al., 2014a; etc.) in the past 20 years. Forster et al. (2007)
51 simulated the global mean direct radiative forcing of total aerosols and BC, which ranges between
52 +0.04 and -0.63 W m^{-2} and between +0.1 and +0.3 W m^{-2}, respectively. Over East Asia, the simulated
53 BC direct raidative forcing varies from +0.32 to +0.81 W m^2 (Zhuang et al., 2013a). All above showed
54 significant uncertainties in estimating the aerosol direct radiative forcing in numerical models. These
55 uncertainties are mostly due to the uncertainties in the aerosol optical properties (Holler et al., 2003)
56 which are related to the aerosol emissions, profiles, compositions and mixing states. Forster et al. (2007)
57 stated that the uncertainties could be reduced if observed aerosol optical properties were employed
58 when estimating the forcing. China has experienced rapid population and economic growth during the
59 past three decades, resulting in enhanced aerosol and trace gas emissions. Streets et al. (2001)
60 suggested that the BC emissions in China roughly accounts for one-fourth of the global anthropogenic
61 emissions, although the uncertainty of this estimate is large. The BC aerosols are mostly emitted in
62 Southwest, North China, Yangtze River Delta (YRD) and Pearl River Delta (PRD) regions (Zhang et al.,
63 2009). Recently, many observation-based studies were conducted on the aerosol optical properties and
64 direct radiative forcing over China (Xu et al., 2004; Yan, 2006; Xia et al., 2007; Yan et al., 2008; He et
65 al., 2009; Wang et al., 2009; Wu et al., 2009; Li et al., 2010; Cai et al., 2011; Bai et al., 2011; Xiao et al.,
66 2011; Zhou et al., 2011; Wu et al., 2012; etc.). Some of them focused on the total extinction or optical
67 depth of the aerosols. Xia et al. (2007) reported that the annual mean optical depth (AOD) at 500 nm
68 and Angstrom exponent (AE) of total aerosols in YRD were 0.77 and 1.17, respectively. Xiao et al.

(2011) analyzed the temporal and spatial variations of the total aerosol optical depth and Angstrom exponent using CE-318 in Hangzhou. Zhuang et al. (2014a) suggested that column AOD and AE of absorbing aerosols were 0.04±0.02 and 1.44±0.50 in urban Nanjing. The aerosol absorption coefficients (AAC) were also studied for several urban and rural areas of China. AAC at 565 nm in Gobi desert was found to be as low as 6 ± 11 Mm^{-1} (Yulin) (Xu et al. 2004). The annual 532 nm-AAC was about 17.54 ± 13.44 Mm^{-1} at a rural site while it was about 45 ± 39 Mm^{-1} at an urban site, in Beijing (Yan et al. 2008; He et al. 2009). AAC at 532 nm was as large as 82 ± 23 Mm^{-1} at urban areas of Pearl River Delta (PRD) in South China (Wu et al. 2009).

Although considerable research on this issue has been conducted, there are still insufficient studies on regional scale in China, especially on AAC in YRD, one of the fastest growing regions in China. To fill the research gaps, this study is to characterize AAC in YRD using the near-surface absorption coefficient and Angstrom exponent of absorbing aerosols in urban Nanjing, a typical developing city in west Yangtze River Delta of China. In the following, the method is described in Section 2. Results and discussions are presented in Section 3, followed by Conclusions in Section 4.

2 Methodologies

2.1 Sampling station and instruments

Sampling site is located in the Gulou campus of Nanjing University, urban Nanjing (32.05^{o} N, 118.78^{o} E). It is built on the roof of a 79.3 m-tall building, around which there are no industrial pollution sources within a 30 km radius but there are several main roads with apparent traffic pollution. The sketch map of the site (not shown) can be referred to Figure 1 of Zhu et al. (2012). The black carbon aerosol mass concentration and aerosol absorption coefficient were derived from the

measurements using the 7-channel Aethalometer (model AE-31, Magee Scientific, USA). The AE-31 model measures light attenuation at seven wavelengths (370, 470, 520, 590, 660, 880, and 950 nm, respectively). The aerosol inlet is located ~1 m above the roof. Routine flow calibration and blank tests were performed before sampling. Details on the AE-31 and its sampling principles can be referred to Hansen et al. (1984), Weingartner et al. (2003) and Arnott et al. (2005). Near-real-time continuous measurements were made at the site since 1 January 2012, using the AE-31, with a desired flow rate of 5.0 L/min and a sampling interval of 5 min. Two-year's data in 2012 and 2013 are used in this study. Meteorological data are from the National Meteorological Station of Nanjing (No. 58238).

2.2 Calculation of AE-31_absorption coefficient

The absorption coefficient is defined with Beer-Lambert's law as shown in Eq. 1 in Weingartner et al. (2003) and Arnott et al. (2005), which is associated with the intensities of the incoming light and remaining light after passing through a medium. A variable ATN, which is given as percentage value, is defined to represent filter attenuation through the sample spot in the tape (Eq. 2 in Weingartner et al., 2003 and Arnott et al., 2005) inside the instrument. Aerosol light absorption coefficient and BC mass concentration can be calculated directly based on the measured light attenuation through a quartz filter matrix. There are two ways in calculating aerosol light absorption coefficient. The indirect calculation (IDC for short), which is much simpler than the direct ones, is expressed as Eq. 1.

$$\sigma_{\mathrm{abs},t}(\lambda) = [BC] \times \gamma \quad (1)$$

where, [BC] is the mass concentration of Aethalometer BC (in μg/m^3) without any correction and γ is the conversion factor determined empirically from linear regression of the Aethalometer BC

concentration versus the aerosol absorption measurement (Yan et al., 2008). Wu et al. (2009) indicated that the conversion factor γ from the linear regression of the Aethalometer BC concentrations (ng/m^3) at 880 nm against the light absorption coefficient (Mm^{-1}) at 532 nm in South China was about 8.28 m^2/g. γ=11.05 m^2/g in the suburb of Nanjing.

In addition to the indirect way, wavelength-depended aerosol absorption coefficient can be calculated directly based on the measured light attenuation (ATN) at seven wavelengths (370, 440, 520, 590, 660, 880 and 950 nm) as shown in Eq. 2:

$$\sigma_{\mathrm{ATN},t}(\lambda)=\frac{(\mathrm{ATN}_t(\lambda)-\mathrm{ATN}_{t-1}(\lambda))}{\Delta t}\times\frac{A}{V} \quad (2)$$

where, A (in m^2) is the area of the aerosol-laden filter spot, V is the volumetric sampling flow rate (in L/min) and Δt is the time interval (=5 min) between t and $t-1$. It is well known that σ_{ATN} is generally larger than the actual aerosol absorption coefficient σ_{abs} because of the optical interactions of the filter substrate with the deposited aerosol (Petzold et al., 1997; Weingartner et al., 2003; Arnott et al., 2005; Schmid et al., 2006). The key factors leading to the bias include: 1) multiple scattering of light at the filter fibers (multiple scattering effect), which may result in the overestimation of the σ, and 2) instrumental response with increased particle loading on the filter (shadowing effect), which may lead to underestimation of the σ. Therefore, the calibration factors *C* and *R* (shown in Eq. 3) are introduced to address the scattering effect and shadowing effect, respectively:

$$\sigma_{\mathrm{abs},t}(\lambda)=\frac{\sigma_{\mathrm{ATN},t}(\lambda)}{C\times R} \quad (3)$$

To address the uncertainties, several correction algorithms, including Weingartner (Weingartner et al., 2003), Arnott (Arnott et al., 2005), Schmid (Schmid et al., 2006), Virkkula (Virkkula et al., 2007) corrections, have been developed. Collaud Coen et al. (2010) suggested that both Weingartner (WC2003 for short, hereinafter) and Schmid (SC2006 for short, hereinafter) corrected-absorptions have

good agreements with the one from Multi-Angle Absorption Photometer. Therefore, these two corrections, which have similar formula shown in Eq. 4, are applied in this study to investigate the absorption coefficient:

$$\sigma_{\mathrm{abs},t}(\lambda)=\frac{\sigma_{\mathrm{ATN},t}(\lambda)}{C\times((\frac{1}{f}-1)\times\frac{\ln(\mathrm{ATN}_t(\lambda))-\ln 10}{\ln 50-\ln 10}+1)} \tag{4}$$

Both of them have the same $R(\lambda)$:

$$R_t(\lambda)=(\frac{1}{f}-1)\times\frac{\ln(\mathrm{ATN}_t(\lambda))-\ln 10}{\ln 50-\ln 10}+1 \tag{5}$$

And R =1 when $\mathrm{ATN}\le 10$. f can be calculated according to Weingartner et al. (2003):

$$f(\lambda)=n\times(1-\omega(\lambda))+1 \tag{6}$$

Where ω is the wavelength depended single scattering albedo (SSA) and n is a constant (=0.86 ± 0.01). Note that the reliability of n value (0.86) is limited because this value is mostly estimated under the condition of $\omega<0.6$, which may result in large bias. Therefore, an empirical f =1.2 (when $\omega\simeq 0.9$), which is independent of wavelength as suggested by Schmid et al. (2006), is used for both WC2003 and SC2006 in this study.

The multiple-scattering correction in WC2003 is also different from that in SC2006. Weingartner (Weingartner et al., 2003) indicated that the two waveband (450 and 660 nm) averaged C was about 3.6 for non-fresh soot. In this study, C in WC2003 is independent of wavelength and is set 3.48 for China according to Wu et al. (2013). In contrast, Schmid (Schmid et al., 2006) pointed out that C, which is wavelength depended, is initially expressed as following:

$$C(\lambda)=C^{*}(\lambda)+m_s(\lambda)\times\frac{\omega(\lambda)}{1-\omega(\lambda)} \tag{7}$$

where m_s represents the fraction of the aerosol scattering coefficient and ω is SSA. Optical

properties from CE-318 were used in this study because there was no concomitant scattering measurements at the site during the whole sampling period. Thus, we assumed that SSA and Angstrom exponent (AE) at the low layers of atmosphere were equated to the column ones. According to Zhuang et al. (2014a), annual mean $\omega(440)$=0.922, $\omega(675)$=0.924, and $\alpha_{a,675/440nm}$=1.44 at the site. Based on $\alpha_{a,675/440nm}$ and according to the definition:

$$\omega(\lambda)=\frac{\sigma_s(\lambda)}{\sigma_s(\lambda)+\sigma_a(\lambda)} \tag{8}$$

$\alpha_{s,675/440nm}$ can be calculated as the following (Angstrom. 1929):

$$\alpha_{s,675/440nm}=-\frac{\log(\frac{\sigma_s(675)}{\sigma_s(440)})}{\log(675/440)}=-\frac{\log(\frac{1-\omega(440)}{\omega(440)}\times\frac{\omega(675)}{1-\omega(675)})}{\log(675/440)}+\alpha_{a,675/440nm} \tag{9}$$

Thus, $\alpha_{s,675/440nm}$=1.51.

All wavelength-depend SSAs could be calculated based on the following formula (Schmid et al., 2006):

$$\omega(\lambda)=\frac{\omega_0\times(\frac{\lambda}{\lambda_0})^{-\alpha_s}}{\omega_0\times(\frac{\lambda}{\lambda_0})^{-\alpha_s}+(1-\omega_0)\times(\frac{\lambda}{\lambda_0})^{-\alpha_a}} \tag{10}$$

Here, ω_0, λ_0, and $\alpha_{s,675/440}$ were set to 0.922, 440 nm and 1.51, respectively. Based on the given $C^*(\lambda)$ and $m_s(\lambda)$ in Table 1 of Arnott et al. (2005), $C(\lambda)$ of pure candle light soot was estimated. To parameterize the dependence among $C(\lambda)$, λ and α_a, $\ln(C)$ versus $\ln(\lambda)$ for α_a=1, 1.5, 2 and 2.5 were plotted in Figure 1 and a quadratic fit (universal formula as shown in Eq. 11) for each α_a value was made following Schmid (Schmid et al., 2006) who suggested that the fits in Figure 1 were applicable to other kind of soot based on given ω and α_s.

$$\ln(C(\lambda))=A\times\ln(\lambda)^2+B\times\ln(\lambda)+D \tag{11}$$

174 Eq. 11 can be transformed into:

175 $$C(\lambda) = C_{ref} \times \frac{\lambda^{A\times\ln(\lambda)+B}}{\lambda_{ref}^{A\times\ln(\lambda)+B}} \quad (12)$$

176

177 α_a-depended A and B are shown in the quadratic equations of Figure 1. A and B versus α_a

178 are shown in Figure 2 and a quadratic fit is made based on the given ω and α_s at our site for A

179 and B individually shown as Eq. 13 and Eq. 14.

180 $$A = 0.123\times\alpha_a^2 - 0.128\times\alpha_a - 0.195 \quad (13)$$

181 $$B = -1.512\times\alpha_a^2 + 1.774\times\alpha_a + 2.637 \quad (14)$$

182

183 Based on Eq. 12, 13 and 14, $C(\lambda)$ at our site could be estimated for a given α_a and C_{ref}.

184 Schmid et al. (2006) indicated that C_{ref} at 532 nm is about 2.1 and 4.0 for pure or external mixtures

185 of soot and internal mixtures of soot, respectively. For the urban aerosols, the mean value 3.6 (Schmid

186 et al., 2006) was suggested and used in this study. Thus C was 2.95, 3.37, 3.56, 3.79, 3.99, 4.51 and

187 4.64 at 370, 470, 520, 590, 660, 880, and 950 nm, respectively.

188 As indicated in Coen et al. (2010), Virkkula correction and Arnott correction are not recommended

189 to be used to correct the absorption coefficient because the Virkkula correction does not consider all the

190 known artifacts and Arnott correction has technical limits due to the generation of new negative

191 absorption coefficient values. Although the determination of the *f* constant used in the WC2003 is not

192 clearly defined, it still shows a very good agreement with the Multi-Angle Absorption Photometer.

193 Similar to Arnott correction, SC2006 also introduces artifacts in the absorption wavelength dependence,

194 but to a lesser extent. And it also shows a very good agreement with the Multi-Angle Absorption

195 Photometer (Coen et al., 2010). Therefore, to estimate absorption coefficient of the aerosol in urban

196 Nanjing, both direct and indirect ways introduced above were employed in this study although the
197 indirect way could only address σ_{abs} at 532 nm. To make the comparison, 532 nm-σ_{abs} from
198 WC2003 and SC2006 was derived using the 520 and 590 nm-σ_{abs} according the following equations
199 (Angstrom. 1929):

200 $$\alpha_{abs,590/520nm} = -\frac{\log(\sigma_{abs,590nm} / \sigma_{abs,520nm})}{\log(590_{nm} / 520_{nm})} \quad (15)$$

201 $$\sigma_{abs,532nm} = \sigma_{abs,520nm} \times (\frac{532_{nm}}{520_{nm}})^{-\alpha_{abs,590/520nm}} \quad (16)$$

202

203 **3 Results and discussion**

204 **3.1 Temporal variations of the aerosol absorption coefficient**

205 We corrected the aerosol absorption coefficient (AAC) in urban Nanjing during the period from
206 2012 to 2013, using three methods: an indirect correction (IDC), Weingartner et al. (2003) (WC2003)
207 and Schmid et al. (2006) (SC2006). It is worth noting that the indirect correction could only estimate a
208 single wavelength AAC (at 532 nm). To make the corrections comparable, 532 nm-AACs from
209 WC2003 and SC2006 were calculated by Eq. 15 and Eq. 16. Temporal variations of AACs for the rest
210 of wavelengths from WC2003 and SC2006 corrections are similar to those of 532 nm-AAC (not
211 shown).

212 Figure 3 presents the monthly variations of 532 nm-AAC in urban Nanjing in 2012 (Figure 3a)
213 and 2013 (Figure 3b) corrected by IDC, WC2003 and SC2006. The seasonal variations and the
214 magnitude of AAC at 532 nm agree closely between the direct and indirect corrections. The relatively
215 large difference in AACs between the direct and indirect corrections was in spring and summer (wet
216 seasons) both in 2012 and 2013. The difference is mostly caused by the shadowing effect *R* because

[BC] directly from AE-31 in Eq. 1 has not been corrected. The bias of the actual BC concentration from [BC] is from the *R* as suggested by Eq.7 in Schmid et al. (2006) and Eq. 7 in Weingartner et al. (2003). Thus, the results imply the importance of the shadowing effect in estimating AACs. The 2-year mean of AAC at 532 nm averaged from the three corrections is about 43.23±28.13 Mm^{-1}, with a maximum and a minimum of 273 Mm^{-1} and 1.28 Mm^{-1}, respectively. AAC at 532 nm corrected by IDC is the largest (44.38 Mm^{-1}), followed by that from WC2003 (43.38 Mm^{-1}) and SC2006 (41.93 Mm^{-1}). AACs in 2012 were a little smaller than those in 2013. The AAC in urban Nanjing had an evident seasonal variation in both 2012 and 2013, generally high in cold seasons and mostly low in warm seasons. Both precipitations and BC emissions may somewhat influence the seasonal variations in the AAC. In summer, high frequent precipitation and low BC emissions (Zhang et al., 2009) result in low BC concentrations, which is opposite to those in winter as suggested by Zhuang et al. (2014b). Additionally, serious pollution episodes would lead to high levels of BC loadings, thus considerably enhancing AACs. Although AACs are generally expected to be small in summer due to low BC concentrations, AAC in June 2012 was substantially large (Fig. 3a). The monthly mean AAC in this month from SC2006 is 51.89 M m^{-1}, which is about 1.5, 1.4 and 1.8 times to that in June of 2012, in summer of 2012 and 2013, respectively. Such high AAC values are mainly resulted from a seriously polluted event of BC during the period from 1st to 15th of June 2012. High BC loadings during this period were due to a high intensity of biomass burning in northwestern region of Nanjing (Zhuang et al. 2014b). Fig. 3 shows that the monthly variation of AAC in 2012 was different from that in 2013. The highest AACs were in June and October 2012 while in 2013, AAC was at the maximum in winter (January, November and December). The large differences between the two years may be due to the difference in pollution episodes, which eventually results in different seasonal variations of AACs in Fig. 3.

AAC also has substantial diurnal variations (Figure 4). It was high at rush hours (around 7-9 o'clock am and pm) but low in afternoon (around 1-3 o'clock pm) almost in all seasons in urban Nanjing in 2012 and 2013. At 7 o'clock am, mean 532 nm-AAC was as large as about 50 Mm^{-1}, while at 2 o'clock pm, it was about 33 Mm^{-1}. The large AACs during the periods of a day might be caused by the vehicle emissions (because the site is surround by several main roads with apparent traffic pollution as mentioned in Section 2) while the small AACs in the afternoon is induced by well developed boundary layer (Zhuang et al. 2014b). Because the diurnal variations of AAC at 532 nm from IDC, WC2003 and SC2006 are similar (Fig 4a), one of them (SC2006) was selected to characterize the AAC's diurnal variation in detail (Fig. 4b). AAC's diurnal variation shows much stronger seasonality in 2013 than that in 2012 (Fig. 4b), which might be caused by substantial pollution episodes discussed above. In 2012, highly intensified biomass burning in early June near Nanjing resulted in higher BC concentrations (Zhuang et al., 2014b) and thus a larger AAC than those in 2013. Extremely high AAC in winter of 2013 might also result from the poor air quality during the period. The diurnal cycle could also deviate from its normal pattern (peak at rush hours and trough in afternoon). Fig. 4b also shows that the standard deviations of AAC in 2012 (25.12 Mm^{-1}) are smaller than those in 2013 (28.58 Mm^{-1}) although their means in 2012 and 2013 are close to each other.

3.2 Frequencies of the aerosol absorption coefficient

Similar to the seasonal variation, the frequency patterns of AACs for the rest of wavelengths are consistent to those of 532 nm-AAC so the following discussion is focused on the frequency of 532 nm-AAC only to avoid duplication. Figure 5a shows the frequency distributions of 532 nm-AAC

corrected by IDC, WC2003 and SC2006 during the study period, following a typical lognormal pattern. The range from 15 to 65 Mm^{-1} dominated, accounting for more than 72% of the total data samples during the period. The maximum frequencies of 10.07% (IDC), 10.57% (WC2003), and 10.89% (SC2006) occurred in the ranges from 25 to 30 Mm^{-1}. The absolute differences between the directly and indirectly corrected AACs were relatively larger in the range from 20 to 25 Mm^{-1} than those in other ranges, possibly due to the influence of the shadowing effect in warming seasons as analyzed in Section 3.1. Because of the consistencies in the frequency patterns and magnitudes among the three AACs, only the frequency of SC2006 AAC at 532 nm is presented in detail to illustrate the inter-annual and seasonal variations of the frequency (Fig. 5b and Fig. 5c). Similar to the diurnal cycle, frequency distributions of AAC in 2012 are more consistent with each other and more concentrated than those in 2013. Frequencies in the ranges below 25 Mm^{-1} (28.57%) and above 70 Mm^{-1} (10.62%) are smaller in 2012 compared to 2013 (31.09% and 15.47%, respectively). The peak frequency mostly occurs in the smaller AAC range in summer while in the larger ones in other seasons. Additionally, pollution episodes might alter the shape of the frequencies especially on seasonal or monthly scales. High aerosol loadings and its AACs would be observed during the episodes, which lead to relatively higher frequency at the larger AACs. As shown in Fig. 5c, frequencies of values exceeding 65 Mm^{-1} were larger in fall compared to those in other seasons in 2012. Frequencies of the values larger than 55 Mm^{-1} were higher in winter compared to those in other seasons in 2013. In 2012, frequency of AAC ranging from 120 to 140 Mm^{-1} in summer was larger (0.94%) than that in spring (0.65%) and winter (0.58%) due to the biomass burning in northwestern regions of Nanjing (Zhuang et al., 2014b). Over all, frequencies of AAC in 2013 show much more seasonality compared to 2012. Large differences in the frequency distribution between 2012 and 2013 are mainly found in summer and winter.

283

284 **3.3 Periodic variation of the aerosol absorption coefficient**

285 In addition to diurnal cycles, AAC in Nanjing might have other periodicities during the study
286 period. Thus, Morlet wavelet is employed based on daily mean values of AAC at 532 nm corrected by
287 SC2006. Figure 6 shows the wavelet power spectrum (Figure 6a) and wavelet real part spectrum
288 (Figure 6b) of 532 nm-AAC. Cycles of 4-8 days and 9-17 days which are mostly statistically
289 significant at the confidence level of 95% dominate the local power spectrum, implying that variations
290 of AAC in urban Nanjing could also be affected by synoptic scale (weekly) weather systems and
291 quasi-two-week scale systems to some extent. The oscillations of AAC on the synoptic scale are found
292 in the period from late fall to early winter due to the quick and vigorous weather change. And
293 quasi-two-week scale oscillations of AAC are mainly in winter. Similar to AAC, visibility in Nanjing
294 also has synoptic scale and quasi-two-week scale periodic variations as indicated in Deng et al. (2011),
295 who suggested that the quasi-two-week oscillation might be a regional rather than local phenomenon in
296 China even in East Asia.

297

298 **3.4 Varied with wavelength of the aerosol absorption coefficient**

299 In the previous sections, single wavelength AAC (at 532 nm) is discussed as the AAC distribution
300 and seasonal variation are similar among different wavelengths. In this section, we further examine
301 wavelength dependent AACs as well as absorption angstrom exponents (AAE) at 660/470 nm corrected
302 by WC2003 and SC2006 (Fig. 7). AACs from both WC2003 and SC2006 decrease with increasing
303 wavelength (Fig. 7a). Although AAC at 532 nm from WC2003 is close to that from SC2006,
304 substantial differences exist at other wavelengths. WC2003-AACs are smaller than SC2006-AACs at

305 shorter wavelengths (370 and 470 nm) but are larger than SC2006-ACCs in longer wavelengths (from
306 590 nm to 950 nm). The averaged AACs range from 23.40 (at 950 nm) to 68.89 Mm^{-1} (at 370 nm)
307 based on WC2003 and range from 17.56 (at 950 nm) to 82.07 Mm^{-1} (at 370 nm) based on SC2006.
308 Different correction methods on scattering effect C between WC2003 and SC2006 result in different
309 variations of AAC with wavelengths because C in WC2003 is independent of wavelength, and
310 subsequently might lead to considerably different AAEs between these corrections (Fig. 7b and 7c).
311 Both Fig. 7b and 7c show that AAE at 660/470 nm from SC2006 is much larger than that from
312 WC2003, although they have similar seasonality. Annual mean 660/470 nm AAEs in 2012 and 2013
313 are 1.58 and 1.54 from SC2006 and 1.09 and 1.07 from WC2003. AAE from SC2006 is about 1.5 times
314 to that from WC2003. Furthermore, AAE has strong seasonality, high in winter and low in summer,
315 implying that absorbing aerosols in summer have larger sizes possibly caused by large relative
316 humidity (RH). Seasonal variations of AAE from AE-31 are similar to those from CE-318 as compared
317 with those in Zhuang et al. (2014a), who reported annual mean AAE of the column aerosols from
318 CE-318 being 1.44 at the site. Thus suggests that the scattering correction method by Schmid et al.
319 (2006) were more reasonable than that by Weingartner et al. (2003).
320
321 Table 1 summaries the optical properties of absorbing aerosols from AE-31 based on IDC,
322 WC2003 and SC2006. Two-years averaged values of AAC at 532 nm corrected by these three methods
323 are 44.38, 43.38 and 41.93 Mm^{-1}, respectively, in urban Nanjing. 660/470 nm AAE corrected by
324 WC2003 and SC2006 are 1.08 ± 0.20 and 1.56 ± 0.23, respectively. Annual mean AAC averaged from
325 all wavelengths is 40.78 Mm^{-1} (SC2006) and 41.41 Mm^{-1} (WC2003), while it is 41.47 Mm^{-1} (SC2006)
326 ~ 42.97 Mm^{-1} (WC2006), averaged from visible wavelengths. The inter-annual difference suggests that

AAC in 2012 is smaller than that in 2013, while AAE in 2012 is larger than that in 2013. The scattering correction of Weingartner et al. (2003) is different from that of Schmid et al. (2006), which would result in large variances of AAC at shorter (<520 nm) or longer (>590 nm) wavelengths, causing large difference of AAE between the two methods. However, AACs at 532 nm or averaged from all wavelengths from WC2003 and SC2006 are close to each other. Many studies on aerosol optical properties have been carried out by model simulations and observations. Most of them focused on the optical depth and single scattering albedo of column (from surface to the top of the atmosphere) aerosols (Zhuang et al., 2014a), few on the aerosol absorption coefficient, even less on AAC in urban areas of YRD. Annual AAE at 660/470 nm corrected by SC2006 agree well with the one observed by CE-318 at the site. Xu et al. (2004) pointed out that AAC at 565 nm was 6 ± 11 Mm^{-1} in Gobi desert (Yulin) in China in 1999. In Beijing, capital of China, annual AAC at 532 nm was about 17.54 ± 13.44 Mm^{-1} at a rural site (Shangdianzi: SDZ) in 2003 and 2004 (Yan et al., 2008) while it was about 45 ± 39 Mm^{-1} at an urban site from 2005 to 2006 (He et al., 2009). AAC at 532 nm at rural site of YRD (Lin'an) was about 44.3 ± 19.7 Mm^{-1} in 2004 (Yan, 2006). In the semi-arid area in Northeast China (Tongyu), AAC at 520 nm was only about 7.28 ± 5.87 Mm^{-1} from 2010 to 2011 (Wu et al., 2012). In Pearl River Delta (PRD) of China, annual AAC at 532 nm was as large as 82 ± 23 Mm^{-1} at urban areas from 2004 to 2007 (Wu et al., 2009). The magnitude of the annual AAC in urban Nanjing, to some extent, is comparable to that in other Chinese urban or rural sites. It is much lower than those in PRD but higher than those in non-urban sites of North China (Shangdianzi, Tongyu and Yulin). In YRD, annual AAC in urban Nanjing is as large as that in rural areas (Lin'an), which is similar to the BC concentrations there (Zhuang et al., 2014b).

3.5 Aerosol absorption coefficient in different wind directions

In addition to local emissions, the meteorological factors such as the prevailing wind could also affect the AAC and AAE in urban Nanjing. Backward trajectories analysis shown in Fig. 8a and 8b indicate that Nanjing could be affected by local air flow and long-distance air flows mostly from northwestern, northern, eastern, southeastern and southern direction both in 2012 and 2013, implying that the prevailing winds might have weaker inter-annual variations than the aerosols. Air flows from northern directions account for about the half of the totals while the local air flow and the flows from the oceans account for about 13%, ~19% and 15%, respectively. Frequencies of air flows from south and northwest China are relatively smaller. The rose plot of near surface wind around the site (32^{o} N, 118.76^{o} E, 8 m tall) during the entire study period (Fig. 8c) suggests that the distributions of the near surface wind directions somewhat agree with those from the backward trajectory analysis. However, the winds near the surface come from the southeastern to eastern directions more frequently, accounting for more than 35% of the totals. The wind from south to west appears the least (Fig. 8c). The wind speed is mostly concentrated in the values from 2 to 6 m/s in Nanjing during the period.

As mentioned, wind direction shifting over different seasons might be another important factor in determining the aerosol AAC and AAE. Zhuang et al. (2014b) indicated that high BC loadings in fall and summer of 2012 were observed at the site when winds were from northeastern and northwestern directions, in which air masses might be highly polluted, thus leading to considerably large AAC. Figure 9 presents the AAC at 532 nm and AAE at 660/470 nm corrected by SC2006 associated with different clusters (shown in Figure 8) in urban Nanjing both in 2012 and 2013. Considerable air pollutants are derived from local and sub-regional emissions as presented in cluster 6 (Fig. 9a and 8a)

371 in 2012 and in cluster 3 (Fig. 9b and 8b) in 2013, with averaged values of 56.13 Mm^{-1} and 65.38 Mm^{-1},
372 respectively. Air masses from the oceans and south China (sea) (cluster 7, 8 and 9 in Fig. 8a and 8b)
373 were relatively clean, leading to smaller AACs in Nanjing (Fig. 9a and 9b), with averaged values of
374 33.28 Mm^{-1} in 2012 and 30.1 Mm^{-1} in 2013. The air masses from the remote sites (cluster 2, 3 and 4 in
375 2012 in Fig. 8a and cluster 1, 4 and 5 in 2013 in Fig. 8b) could also bring the clean air and then might
376 result in relatively low levels of AACs in Nanjing. Previous analysis indicates that prevailing winds
377 have weak inter-annual variations. Therefore, substantial differences (about 15 Mm^{-1}) between AAC
378 from cluster 3 (or cluster 5) in 2012 and cluster 2 (or cluster 6) in 2013 might mostly result from the
379 regional pollution episodes in North China in 2013. In addition to AAC, AAE is also somewhat
380 affected by different air flows. Fig. 9c and 9d suggest that AAE in urban Nanjing is relatively small
381 when the air masses come from the oceans (cluster 7 and 9) possibly due to the affection of moisture
382 while is larger when the flows are from the areas of higher latitudes. Local AAEs are 1.52 (in cluster 6
383 in Fig. 9c) in 2012 and 1.62 (in cluster 3 in Fig. 9d) in 2013, which are close to the annual mean value
384 of 1.56.
385
386 **3.6 Relationship between aerosol absorption coefficient and its absorption angstrom exponent**
387 Aerosol absorption coefficient is directly determined by the loadings of absorbing aerosols.
388 Additionally, both aerosol size's distribution and relative humidity (RH), especially the former, are
389 closely related to the variation in AAC. Figure 10 shows the relationships among AAC at 532 nm
390 corrected by SC2006, AAE at 660/470 nm corrected by SC2006 and RH. It suggests that changes in
391 aerosol mass (or specific) absorption coefficients (MAC for short, defined as ratios of AAC to BC
392 loading, in m^2/g) at 532 nm are closely relative to the variations of AAE. High levels of MAC mostly

393 appear in the ranges with large AAE, implying that absorbing aerosols with smaller sizes might absorb
394 more solar radiation because the fine particles have much larger specific surface areas compared to
395 coarse ones. The linear correlation coefficient between MAC and AAE exceeded 0.92 in urban Nanjing
396 during the study period (Fig. 10a). Changes in AAE somewhat are influenced by the variations of RH.
397 Fig. 10a also indicates that large AAEs are mostly found when the RH is low and vice versa. Generally,
398 moist air is in favor of hygroscopic growth of the aerosols, thus resulting in smaller AAE
399 (corresponding to large size of the aerosols). These results could further explain why AAE in urban
400 Nanjing is relatively small when the air masses come from the oceans as discussed in the previous
401 section (Fig. 8 and 9). In addition to AAE, AAC is also affected by RH, as shown in Fig. 10b for
402 AAC-RH relationship in different AAE levels. Large AAC appears in the range with large AAE while
403 coarser aerosols (AAE<1.3) could only be found under the condition of large RH. Changes in AAC
404 with RH are different within different bins of AAE. Polynomial fitting between AAC and RH indicates
405 that the peaks of AAC mainly concentrate at RH being 65% for the finer (AAE>1.6) absorbing aerosols
406 (unimodal). While for coarser ones, quasi-bimodal distribution of AAC is found. High levels of AAC
407 within the ranges of AAE from 1.3 to 1.6 mostly appear at the value of 40% and 80%. Large AACs
408 within the ranges of AAE below 1.3 are mostly found in the value of 65% and 85%. Polynomial
409 correlation coefficients of these three fittings are 0.25, 0.16 and 0.38, respectively, which is statistically
410 significant at the confident levels of 99%, 99% and 90%.
411
412 **3.7 Aerosol absorption coefficient during pollution episodes**
413 The previous analysis indicates that extremely high aerosols were observed from serious pollution
414 episodes, which might affect the temporal and frequency distributions of AAC in urban Nanjing. The

415 diurnal variation of BC in the period from 1st to 15th June in 2012 was altered significantly from its
416 normal distribution (Zhuang et al., 2014b), so does the AAC in this period as expected. The mean of
417 AAC at 532 nm from January 2012 to December 2013 shown in Table 1 is about 43 Mm^{-1}. However,
418 the daily mean AACs far outstripping the value 90 Mm^{-1}, ~2 times of the annual mean, is found
419 frequently, especially in March, June, and November of 2012 and in January, November, and December
420 of 2013 (Figure 11). The largest values of the daily AAC at 532 corrected by SC2006 in these months
421 all exceeded 100 Mm^{-1}, especially on the 10th June 2012 and 4th December 2013 when AACs were as
422 large as 147.19 and 149.38 Mm^{-1}, respectively. The high AAC in June 2012 mainly result from biomass
423 burning in the northwestern region of Nanjing (belongs to local pollution in cluster 6 of Fig. 8a), as
424 discussed in Zhuang et al. (2014b). The magnitude and distribution of Aerosol optical depth (AOD)
425 from satellite (MODIS) retrievals (not shown) suggest that the high aerosol loadings or absorption
426 coefficients during the periods from the 9th to 13th January 2013 and from the 1st to 8th December 2013
427 might be possibly caused by large scale regional pollution over East to North China (Nanjing is
428 included). The reasons leading to high aerosol pollution in Nanjing during the sampling period would
429 be analyzed in detailed in further studies, so does the characteristics of AAC and AAE in pollution
430 episodes.
431
432 **4 Conclusions**
433 In this study, the near-surface aerosol absorption coefficient (AAC) and angstrom exponent (AAE)
434 in urban Nanjing in 2012 and 2013 are investigated based on the measurements from the 7-channel
435 Aethalometer (model AE-31, Magee Scientific, USA). As suggested by Collaud Coen et al. (2010),
436 Weingartner et al. (2003) (WC2003 for short) and Schmid et al. (2006) (SC2006 for short) corrections

437 are used to assess the AAE at 660/470 nm and wavelength depended AAC. The indirect correction
438 (IDC) is also used to estimate the 532 nm-AAC based on the observed conversion factor in Nanjing.
439 Analysis in AAC is focused on at wavelength 532 nm to facilitate the comparisons between the directly
440 and indirectly correction of AACs, as the temporal variation and frequency distribution of ACC at each
441 wavelength are similar to those at 532 nm.

442 The direct and indirect corrections closely agree in terms of the temporal variation and magnitude
443 of AAC at 532 nm in the entire study period except in spring and summer possibly due to the strong
444 shadowing effect in these seasons. AAC at 532 nm corrected by IDC is the largest, followed by that
445 from WC2003 and SC2006. The mean AAC at 532 nm averaged from these three corrections is about
446 43.23±28.13 Mm^{-1} in urban Nanjing, with substantial seasonal and diurnal variations. Higher AACs
447 often appear in cold seasons (at rush hours) while lower ones in summer (in afternoon). Small AAC in
448 summer (in afternoon) is partially due to large scavenging efficiency and smaller emission rates of the
449 aerosols (the well developed boundary layers). AAC in urban Nanjing is much lower than that in Pearl
450 River Delta but higher than that at non-urban sites of North China. Within YRD, annual AAC in urban
451 Nanjing is as large as that in rural areas (Lin'an). Wavelet analysis suggests that variations of AAC in
452 urban Nanjing might have cycles of 4-8 days and 9-17 days due to the affection of synoptic scale
453 (weekly) weather systems and quasi-two-week scale systems. AACs follow a typical lognormal pattern
454 in terms of the frequency distribution. For AAC at 532 nm, the range from 15 to 65 Mm^{-1} dominates,
455 accounting for more than 72% of the total data samples in the entire study period. The maximum
456 frequencies of about 10-11% occur at the ranges from 25 to 30 Mm^{-1}. Both diurnal variations and
457 frequency distributions of AAC shows more evident seasonality in 2013 than those in 2012 possibly
458 because of the influences of the pollution episodes.

AAC in urban Nanjing has been affected by serious pollution episodes locally and regionally, thus much enhanced AACs have been observed frequently. AACs are expected to be small in summer due to low BC concentrations at the time. However, AACs were substantially large (exceeding 50 Mm^{-1}) in June 2012 due to a high intensity of biomass burning around Nanjing during 1-15 June 2012. Extremely high AACs in winter in 2013 might be caused by large scale regional pollutions over East to North China. Hence, AAC diurnal cycle, frequency, and their seasonal variations were altered. High AACs appeared at mid-night during the period 1-15 June 2012, instead of in the morning as usual. Frequency of AAC followed a quasi-bimodal distribution in winter in 2013 and its values at the AAC range larger than 55 Mm^{-1} were higher compared to those in other seasons in 2013.

The AAC at the site generally decreases with increasing wavelength. Although AAC at 532 nm from WC2003 is close to the one from SC2006, its decline rate is smaller than SC2006's because the scattering correction C from WC2003 is independent of wavelength. Thus, AAE at 660/470 nm from SC2006 (=1.56) is much larger than that from WC2003 (=1.08). The scattering correction by Schmid et al. (2006) appears more reasonable than that by Weingartner et al. (2003), compared to the column AAE at 675/440 nm by CE-318 at the site. AAE also has strong seasonality, high in winter and low in summer, possibly related to the variation in relative humidity (RH) (Zhuang et al., 2014a).

Wind direction shifting over different seasons might be another factor controlling the aerosol AAC and AAE. Backward trajectories indicate that Nanjing could be affected by local air flow (13% ~19%) and long-distance air flows mostly from northwestern, northern (>50%), eastern, southeastern and southern directions. Considerable air pollutions in urban Nanjing are due to local and sub-regional emissions. Air masses from the oceans and remote areas are relatively clean with low AACs. During the pollution episodes in North China in 2013, a large number of aerosols were transported to Nanjing,

481 greatly enhancing AAC at the site. AAE at the site is usually low when the air masses come from the
482 oceans while it is high when the air flows from higher latitudes.

483 AAC generally increases with increasing AAE under the condition of fixed aerosol loadings in
484 urban Nanjing. The linear correlation coefficient between aerosol mass absorption coefficients (MAE)
485 at 532 nm and AAC exceeds 0.92 during the entire study period. High levels of MAC mostly appear in
486 the ranges with large AAE because the fine particles have much larger specific surface area compared
487 to coarse ones. Changes in AAE and AAC are somewhat influenced by the variations of RH. Large
488 AAEs are mostly found when the RH is low and vice versa. Changes in AAC with RH are different
489 within different bins of AAE. Unimodal and quasi-bimodal distributions of AAC vary with RH for
490 finer (AAE>1.6) and coarser (AAE<1.6) absorbing aerosols, respectively. The peak AAC mainly
491 concentrates at RH= 65% for the aerosols with AAE<1.6. For the aerosols with 1.3<AAE<1.6, the
492 maximum AACs appear around RH being 40% and 80%, while for AAE<1.3, AAC peaks around RH
493 being 65% and 85%.

494

495 **Acknowledgements:** This work was supported by the National Key Basic Research Development
496 Program of China (2014CB441203 and 2011CB403406), the Young Scientists Fund of the National
497 Natural Science Foundation of China (41205111), the New Teachers' Fund for Doctor Stations,
498 Ministry of Education (20120091120031), the Fundamental Research Funds for the Central
499 Universities (20620140744), FP7 project: REQUA (PIRSES-GA-2013-612671), and a project Funded
500 by the Priority Academic Program Development of the Jiangsu Higher Education Institutions (PAPD).
501 The authors would like to thank all members in the AERC of Nanjing University for maintaining
502 instruments. HYSPLIT model was supplied by NOAA: http://ready.arl.noaa.gov/HYSPLIT_traj.php.

5 References

Angström, A.: On the atmospheric transmission of sun radiation and on dust in the air, Geogr. Ann., 11, 156–166, 1929.

Arnott, W. P., Hamasha, K., Moosmuller, H., Sheridan, P. J., and Ogren, J. A.: Towards aerosol light-absorption measurements with a 7-wavelength aethalometer: evaluation with a photoacoustic instrument and 3-wavelength nephelometer, Aerosol Sci. Tech., 39, 17–29, doi:10.1080/027868290901972, 2005.

Bai, H. T., Chen, Y. H., Wang, H. Q., Zhang, Q., Guo, N., Wang, S., Pan, H., and Zhang, P.: Seasonal variation of aerosol optical properties at AERONET of the semi-arid region in Loess Plateau, Arid Land Geogr., 34, 1–8, 2011.

Bellouin, N., Boucher, O., Tanré, D., and Dubovik, O.: Aerosol absorption over the clear-sky oceans deduced from POLDER-1 and AERONET observations, Geophys. Res. Lett., 30, 1748, doi:10.1029/2003GL017121, 2003.

Cai, H. K., Zhou, R. J., Fu, Y. F., Zheng, Y. Y., and Wang, Y. J.: Cloud-aerosol lidar with or thogonal polarization detection of aerosol optical properties after a crop burning case, Clim. Environ. Res., 16, 469–478, 2011.

Collaud Coen, M., Weingartner, E., Apituley, A., Ceburnis, D., Fierz-Schmidhauser, R., Flentje, H., Henzing, J. S., Jennings, S. G., Moerman, M., Petzold, A., Schmid, O., and Baltensperger, U.: Minimizing light absorption measurement artifacts of the Aethalometer: evaluation of five correction algorithms, Atmos. Meas. Tech., 3, 457–474, doi:10.5194/amt-3-457-2010, 2010.

Deng, J. J., Wang, T. J., Jiang, Z. Q., Xie, M., Zhang, R. J., Huang, X. X., and Zhu, J. L.:

525 Characterization of visibility and its affecting factors over Nanjing, China, Atmos. Res., 101,
526 681–691, doi:10.1016/j.atmosres.2011.04.016, 2011.
527 Forster, P., Ramaswamy, V., Artaxo, P., Berntsen, T., Betts, R., Fahey, D. W., Haywood, J., Lean, J.,
528 Lowe, D. C., Myhre, G., Nganga, J., Prinn, R., Raga, G., Schulz, M., and Van Dorland, R.: Changes
529 in atmospheric constituents and in radiative forcing, in: Climate Change 2007: The Physical
530 Science Basis. Contribution of Working Group I to the Fourth Assessment Report of the
531 Intergovernmental Panel on Climate Change, edited by: Solomon, S. et al., Cambridge Univ. Press,
532 Cambridge, UK, 129–234, 2007.
533 Hansen, A. D. A., Rosen, H., and Novakov, T.: The aethalometer: an instrument for the real time
534 measurements of optical absorption by aerosol particles, Sci. Total Environ., 36, 191–196, 1984.
535 He, X., Li, C. C., Lau, A. K. H., Deng, Z. Z., Mao, J. T., Wang, M. H., and Liu, X. Y.: An intensive
536 study of aerosol optical properties in Beijing urban area, Atmos. Chem. Phys., 9, 8903–8915,
537 doi:10.5194/acp-9-8903-2009, 2009.
538 Holler, R., Ito, K., Tohno, S., and Kasahara, M.: Wavelength-dependent aerosol single scattering albedo:
539 measurements and model calculations for a coastal site near the sea of Japan during ACE-Asia, J.
540 Geophys. Res., 108, 8648, doi:10.1029/2002JD003250, 2003.
541 Jacobson, M. Z.: Control of fossil-fuel particulate black carbon and organic matter, possibly the most
542 effective method of slowing global warming, J. Geophys. Res., 107, 4410,
543 doi:10.1029/2001JD001376, 2002.
544 Kiehl, J. T. and Briegleb, B. P.: The relative roles of sulfate aerosols and greenhouse gases in climate
545 forcing, Science, 260, 311–314, 1993.
546 Li, Z. Q., Lee, K. H., Wang, Y. S., Xin, J. Y., and Hao, W. M.: First observation-based estimates of

547 cloud-free aerosol radiative forcing across China, J. Geophys. Res., 115, D00K18,
548 doi:10.1029/2009JD013306, 2010.
549 Liao, H. and Seinfeld, J. H.: Global impacts of gas-phase chemistry-aerosol interactions on direct
550 radiative forcing by anthropogenic aerosols and ozone, J. Geophys. Res., 110, D18208,
551 doi:10.1029/2005JD005907, 2005.
552 Menon, S., Hansen, J., Nazarenko, L., and Luo, Y. F.: Climate effects of black carbon aerosols in China
553 and India, Science, 297, 2250–2253, doi:10.1126/science.1075159, 2002.
554 Penner, J. E., Andreae, M., Annegarn, H., Barrie, L., Feichter, J., Hegg, D., Jayaraman, A., Leaitch, R.,
555 Murphy, D., Nganga, J., and Pitari, G.: Aerosols, their direct and indirect effects, in: Climate
556 Change 2001: The Scientific Basis. Contribution of Working Group I to the Third Assessment
557 Report of the Intergovernmental Panel on Climate Change, edited by: Houghton, J. T. et al.,
558 Cambridge University Press, Cambridge, UK and New York, NY, USA, 289–348, 2001.
559 Petzold, A., Kopp, C., and Niessner, R.: The dependence of the specific attenuation cross-section on
560 black carbon mass fraction and particle size, Atmos. Environ., 31, 661–672, 1997.
561 Schmid, O., Artaxo, P., Arnott, W. P., Chand, D., Gatti, L. V., Frank, G. P., Hoffer, A., Schnaiter, M., and
562 Andreae, M. O.: Spectral light absorption by ambient aerosols influenced by biomass burning in the
563 Amazon Basin. I: Comparison and field calibration of absorption measurement techniques, Atmos.
564 Chem. Phys., 6, 3443–3462, doi:10.5194/acp-6-3443-2006, 2006.
565 Streets, D. G., Gupta, S., Waldhoff, S. T., Wang, M. Q., Bond, T. C., and Bo, Y. Y.: Black carbon
566 emissions in China, Atmos. Environ., 35, 4281–4296, doi:10.1016/S1352-2310(01)00179-0, 2001.
567 Virkkula, A., Makela, T., Hillamo, R., Yli-Tuomi, T., Hirsikko, A., Hameri, K., and Koponen, I. K.: A
568 simple procedure for correcting loading effects of aethalometer data, J. Air Waste Manage., 57,

569 1214–1222, doi:10.3155/1047-3289.57.10.1214, 2007.
570 Wang, Y., Che, H. Z., Ma, J. Z., Wang, Q., Shi, G. Y., Chen, H. B., Goloub, P., and Hao, X. J.: Aerosol
571 radiative forcing under clear, hazy, foggy, and dusty weather conditions over Beijing, China,
572 Geophys. Res. Lett., 36, L06804, doi:10.1029/2009GL037181, 2009.
573 Weingartner, E., Saathoff, H., Schnaiter, M., Streit, N., Bitnar, B., and Baltensperger, U.: Absorption of
574 light by soot particles: determination of the absorption coefficient by means of aethalometers, J.
575 Aerosol Sci., 34, 1445–1463, doi:10.1016/S0021-8502(03)00359-8, 2003.
576 Wu, D., Mao, J. T., Deng, X. J., Tie, X. X., Zhang, Y. H., Zeng, L. M., Li, F., Tan, H. B., Bi, X. Y.,
577 Huang, X. Y., Chen, J., and Deng, T.: Black carbon aerosols and their radiative properties in the
578 Pearl River Delta region, Sci. China Ser. D, 52, 1152–1163, doi:10.1007/s11430-009-0115-y, 2009.
579 Wu, D.,Wu, C., Liao, B., Chen, H.,Wu, M., Li, F., Tan, H., Deng, T., Li, H., Jiang, D., and Yu, J. Z.:
580 Black carbon over the South China Sea and in various continental locations in South China, Atmos.
581 Chem. Phys., 13, 12257–12270, doi:10.5194/acp-13-12257-2013, 2013.
582 Wu, Y. F., Zhang, R. J., Pu, Y. F., Zhang, L. M., Ho, K. F., and Fu, C. B.: Aerosol optical properties
583 observed at a semi-arid rural site in northeastern China, Aerosol Air Qual. Res., 12, 503–514, 2012.
584 Xia, X. A., Li, Z. Q., Holben, B., Wang, P., Eck, T., Chen, H. B., Cribb, M., and Zhao, Y. X.: Aerosol
585 optical properties and radiative effects in the Yangtze Delta region of China, J. Geophys. Res., 112,
586 D22S12, doi:10.1029/2007JD008859, 2007.
587 Xiao, Z. Y., Jiang, H., Chen, J., Wang, B., and Jiang, Z. S.: Monitoring the aerosol optical properties
588 over Hangzhou using remote sensing data, Acta Sci. Circumst., 31, 1758–1767, 2011.
589 Xu, J., Bergin, M. H., Greenwald, R., Schauer, J. J., Shafer, M. M., Jaffrezo, J. L., and Aymoz, G.:
590 Aerosol chemical, physical, and radiative characteristics near a desert source region of Northwest

591 China during ACE-Asia, J. Geophys. Res., 109, D19S03, doi:10.1029/2003JD004239, 2004.
592 Yan, P.: Study on the aerosol optical properties in the background regions in the East part of China,
593 PhD Thesis, Peking University, China, 2006.
594 Yan, P., Tang, J., Huang, J., Mao, J. T., Zhou, X.J., Liu, Q., Wang, Z. F., and Zhou, H. G.: The
595 measurement of aerosol optical properties at a rural site in Northern China, Atmos. Chem. Phys., 8,
596 2229–2242, doi:10.5194/acp-8-2229-2008, 2008.
597 Zhang, Q., Streets, D. G., Carmichael, G. R., He, K. B., Huo, H., Kannari, A., Klimont, Z., Park, I. S.,
598 Reddy, S., Fu, J. S., Chen, D., Duan, L., Lei, Y., Wang, L. T., and Yao, Z. L.: Asian emissions in
599 2006 for the NASA INTEX-B mission, Atmos. Chem. Phys., 9, 5131–5153,
600 doi:10.5194/acp-9-5131-2009, 2009.
601 Zhou, B., Zhang, L., Cao, X. J., Han, X., Zhang, W., and Feng, G. H.: Analyses on atmospheric aerosol
602 optical properties with lidar data in Lanzhou suburb, Plateau Meteorol., 30, 1011–1017, 2011.
603 Zhu, J., Wang, T., Talbot, R., Mao, H., Hall, C. B., Yang, X., Fu, C., Zhuang, B., Li, S., Han, Y., and
604 Huang, X.: Characteristics of atmospheric Total Gaseous Mercury (TGM) observed in urban
605 Nanjing, China, Atmos. Chem. Phys., 12, 12103–12118, doi:10.5194/acp-12-12103-2012, 2012.
606 Zhuang, B. L., Li, S., Wang, T. J., Deng, J. J., Xie, M., Yin, C. Q., and Zhu, J. L.: Direct radiative
607 forcing and climate effects of anthropogenic aerosols with different mixing states over China,
608 Atmos. Environ., 79, 349–361, doi:10.1016/j.atmosenv.2013.07.004, 2013a.
609 Zhuang, B. L., Liu, Q., Wang, T. J., Yin, C. Q., Li, S., Xie, M., Jiang, F., and Mao, H. T.: Investigation
610 on semi-direct and indirect climate effects of fossil fuel black carbon aerosol over China, Theor.
611 Appl. Climatol., 114, 651–672, doi:10.1007/s00704-013-0862-8, 2013b.
612 Zhuang, B. L., Wang, T. J., Li, S., Liu, J., Talbot, R., Mao, H. T., Yang, X. Q., Fu, C. B., Yin, C. Q.,

613 Zhu, J. L., Che, H. Z., and Zhang, X. Y.: Optical properties and radiative forcing of urban aerosols
614 in Nanjing, China, Atmos. Environ., 83, 43–52, 2014a.
615 Zhuang, B. L., Wang, T. J., Liu, J., Li, S., Xie, M., Yang, X. Q., Fu, C. B., Sun, J. N., Yin, C. Q., Liao, J.
616 B., Zhu, J. L., and Zhang, Y.: Continuous measurement of black carbon aerosol in urban Nanjing of
617 Yangtze River Delta, China, Atmos. Environ., 89, 415–424, 2014b.
618
619 **Figure captions:**
620 Figure 1. Double logarithmic plot of C versus λ for α_a=1 (orange), 1.5 (green), 2 (blue) and 2.5
621 (violet), respectively.
622 Figure 2. Variations of the coefficients A and B with α_a.
623 Figure 3. Monthly variations of the aerosol absorption coefficients (Mm^{-1}) at 532 nm in urban Nanjing
624 in 2012 (a) and 2013 (b). The 10th, 25th, median, 75th, 90th percentile values of the coefficient
625 corrected by SC2006 are presented as box plot. The monthly means of the coefficients corrected by
626 indirect way (red), WC2003 (blue) and SC2006 (light green) are presented as line-markers.
627 Figure 4. Diurnal variations of the aerosol absorption coefficients at 532 nm in urban Nanjing. (a) the
628 two-year (2012-2013) coefficients corrected by indirect way (red), WC2003 (blue) and SC2006 (light
629 green) and (b) the coefficients corrected by SC2006 in separate seasons of 2012 and 2013. Mar, April
630 and May represent the spring, June, July and August represent the summer, September, October and
631 November represent the fall, and January, February and December in 2012 (2013) represent the winter
632 in 2012 (2013).
633 Figure 5. Frequency distributions of the aerosol absorption coefficients at 532 nm in urban Nanjing. (a)
634 the two-year (2012-2013) coefficients corrected by indirect way (red), WC2003 (blue) and SC2006

635 (light green), (b) the coefficients corrected by SC2006 in separate year 2012 (solid bar) and 2013 (erase
636 bar), and (c) the coefficients corrected by SC2006 in separate seasons of separate year.

637 Figure 6. The local wavelet power spectrum (a) and wavelet real part spectrum (b) of the aerosol
638 absorption coefficient at 532 nm using the Morlet wavelet. The left axis is the wavelet scale (in day)
639 corresponding to the Fourier period on the right axis. The bottom axis is local time (month). The filled
640 parts in Fig. 6a indicate passing 95% confidence level test, and the parts below the dashed line are
641 unlikelihood.

642 Figure 7. Dependence of the aerosol absorption coefficient corrected by WC2003 (blue) and SC2006
643 (green) on the wavelength in urban Nanjing during the period from 2012 to 2013 (Fig. a). Annual (dash
644 lines) and seasonal (bars with error bar) absorption angstrom exponents at 660/470 nm from WC2003
645 (light blue) and SC2006 (green) both in 2012 (Fig. b) and 2013 (Fig. c).

646 Figure 8. Clusters of 96-h back trajectories arriving at the study site at 100 m in 2012 (a) and 2013 (b)
647 simulated by HYSPIT model and the probability distributions of 6 hours interval near surface wind
648 speed in different wind directions in Nanjing (c).

649 Figure 9. The 10%, 25%, 50%, 75% and 90% percentile values of the aerosol absorption coefficient (a,
650 b) and absorption angstrom exponent (c, d) in each cluster of back trajectories in 2012 (Fig. 8a) and
651 2013 (Fig. 8b).

652 Figure 10. Relationships between the aerosol mass (or specific) absorption coefficient (m^2/g) and its
653 angstrom exponent (a, scatter plots) and the effects of relative humidity on the aerosol absorption
654 coefficient (a, in color and b) in different absorption angstrom exponent levels.

655 Figure 11. Time series of daily mean aerosol absorption coefficient at 532 nm corrected by IDC (red),
656 WC2003 (blue) and SC2006 (green) in the period from 2012 to 2013.

Tables:

Table 1. Statistical values of annual aerosol absorption coefficient (Mm^{-1}) and absorption angstrom exponent in urban Nanjing

Year	Schemes	All wave AAC		Visible wave AAC		532 nm- AAC		AAE (660/470 nm)	
		Average	Std	Average	Std	Average	Std	Average	Std
2012	IDC	/	/	/	/	42.99	26.55	/	/

	SC2006	39.70	35.26	40.34	27.10	41.02	25.70	1.58	0.20
	WC2003	40.48	31.26	41.97	27.29	42.44	26.59	1.09	0.20
2013	IDC	/	/	/	/	45.81	30.22	/	/
	SC2006	41.91	38.64	42.66	30.61	42.87	29.14	1.54	0.25
	WC2003	42.39	34.41	43.99	30.79	44.34	30.15	1.07	0.21
2-year	IDC	/	/	/	/	44.38	28.45	/	/
period	SC2006	40.78	36.97	41.47	28.89	41.93	27.47	1.56	0.23
	WC2003	41.41	32.86	42.97	29.08	43.38	28.41	1.08	0.20

676 IDC: The coefficients from the indirect correction.

677 SC2006: The coefficients corrected by Schmid et al. (2006).

678 WC2003: The coefficients corrected by Weingartner et al. (2003).

679 AAC: Aerosol absorption coefficients.

680 AAE: Absorption angstrom exponent.

681

682

Figures:

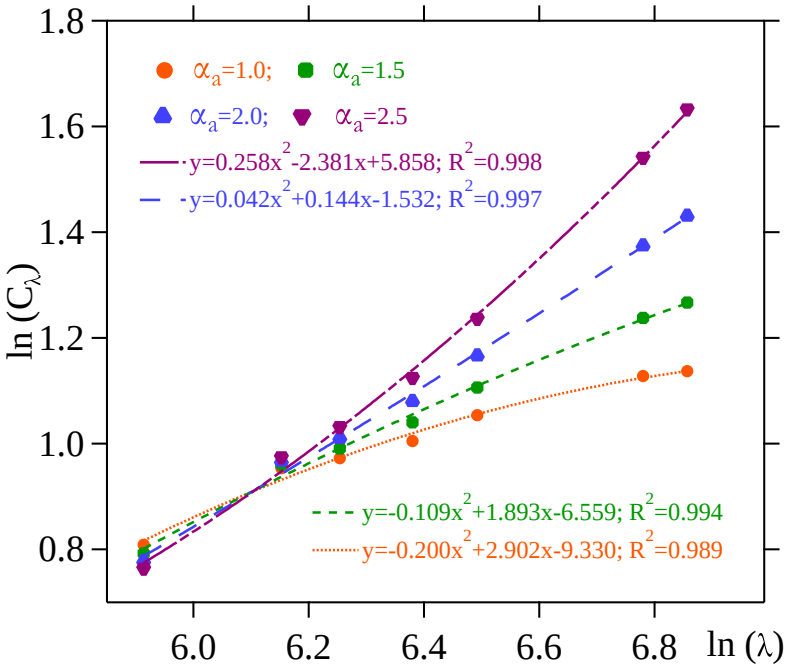

Figure 1.

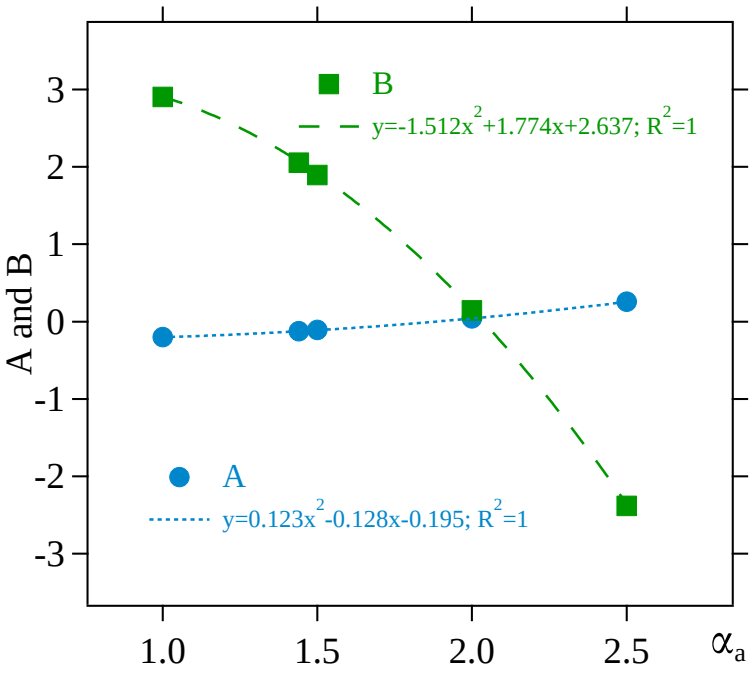

Figure 2.

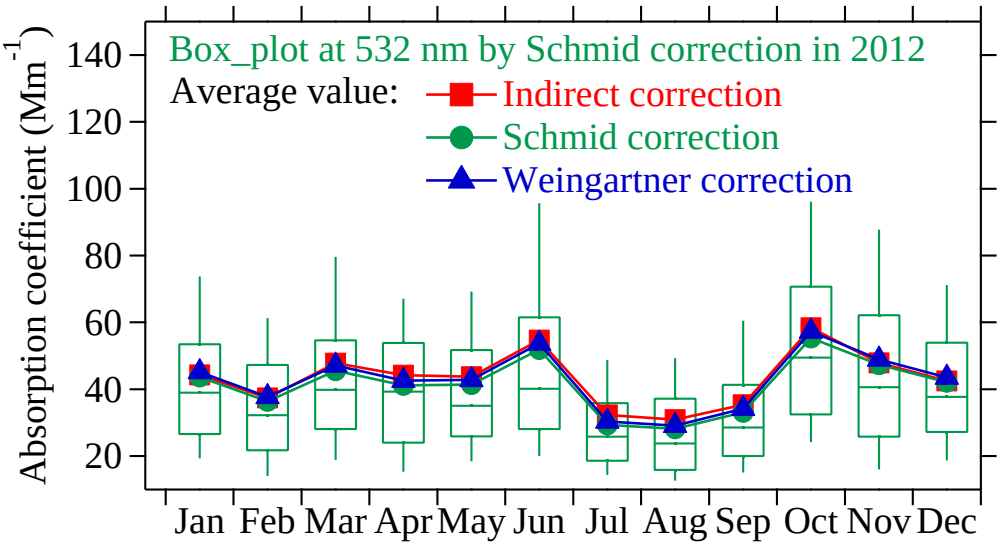
Box_plot at 532 nm by Schmid correction in 2012
Average value:
Indirect correction
Schmid correction
Weingartner correction
Absorption coefficient (Mm-1)
140
120
100
80
60
40
20
Jan Feb Mar Apr May Jun Jul Aug Sep Oct Nov Dec

a)

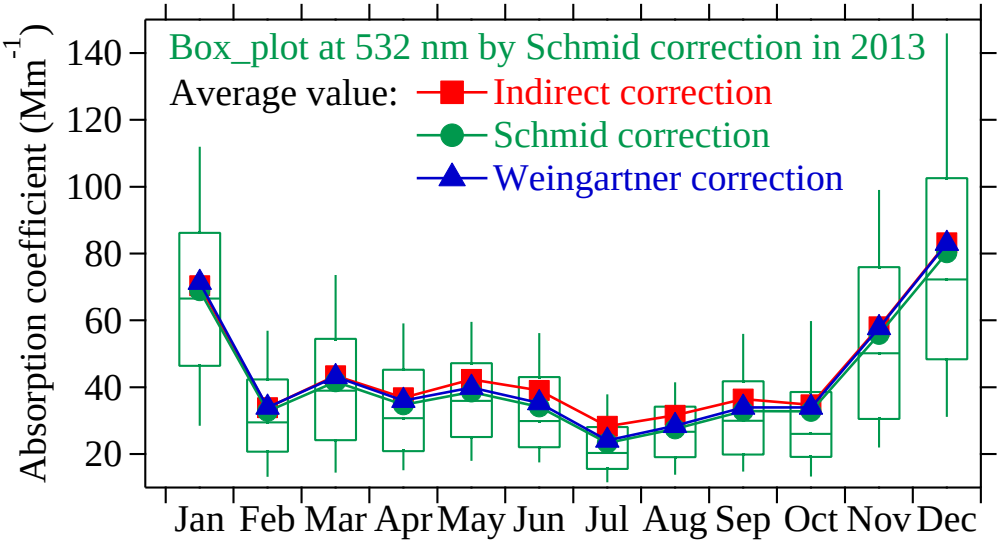
Box_plot at 532 nm by Schmid correction in 2013
Average value:
Indirect correction
Schmid correction
Weingartner correction
Absorption coefficient (Mm-1)
140
120
100
80
60
40
20
Jan Feb Mar Apr May Jun Jul Aug Sep Oct Nov Dec

b)

Figure 3

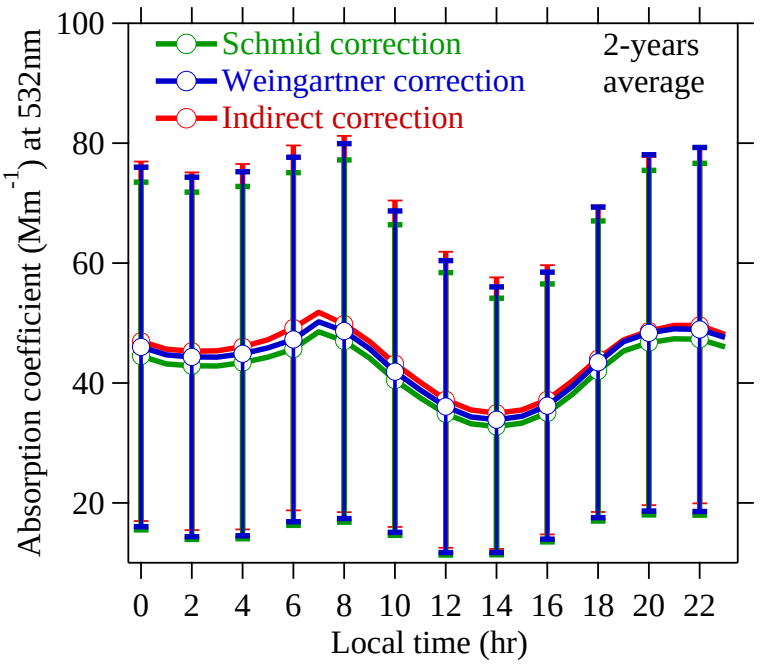
Schmid correction
Weingartner correction
Indirect correction
2-years
average
Absorption coefficient (Mm-1) at 532nm
Local time (hr)

a)

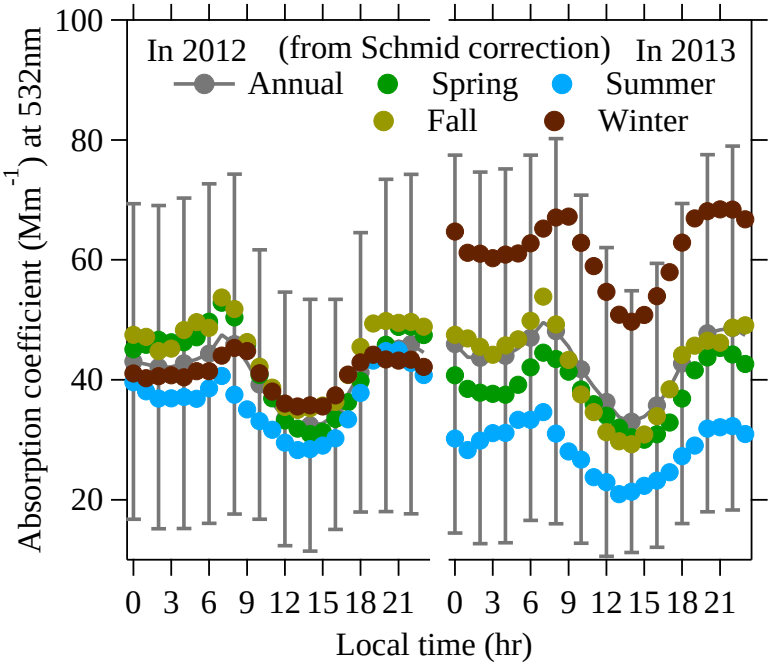
In 2012
(from Schmid correction)
In 2013
Annual
Spring
Summer
Fall
Winter
Absorption coefficient (Mm-1) at 532nm
Local time (hr)

b)

Figure 4

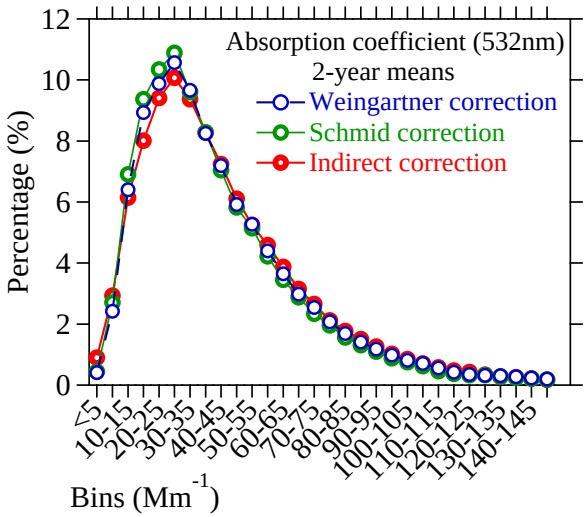

714

715 a)

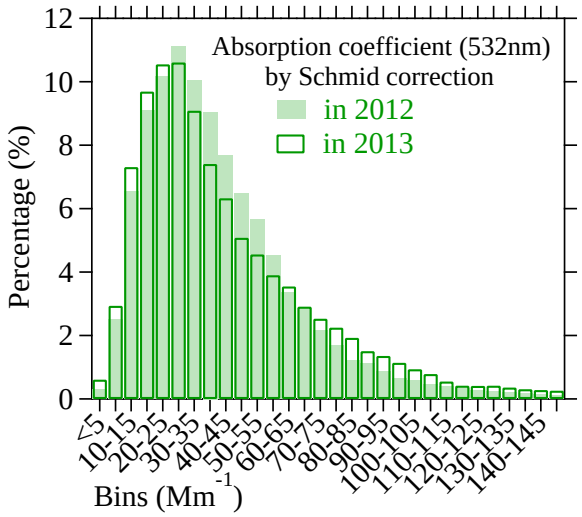

716

717 b)

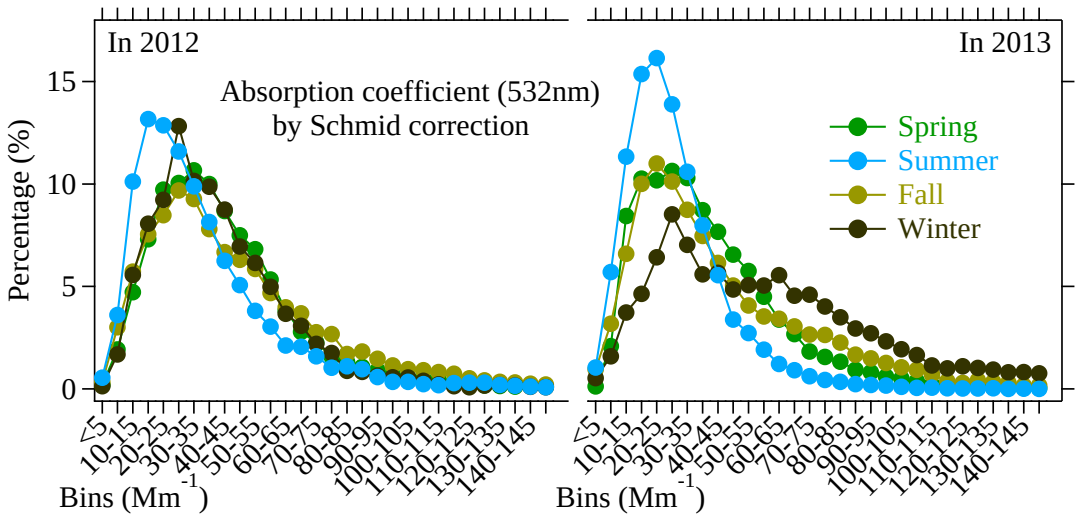

718

719 c)

720 Figure 5

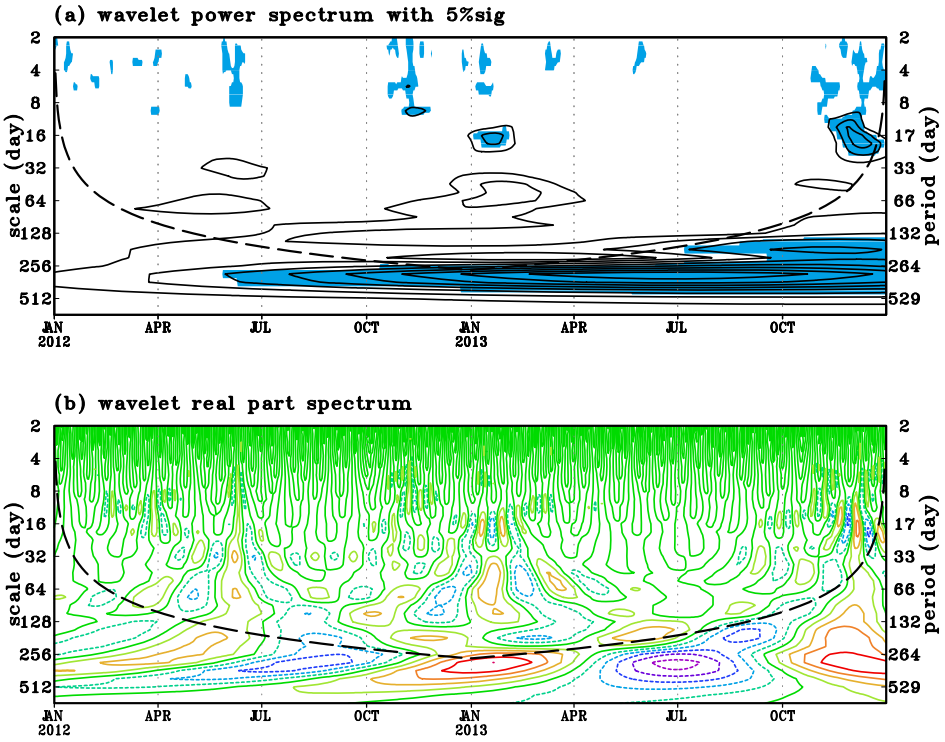
(a) wavelet power spectrum with 5%sig
scale (day)
period (day)
2
4
8
16
32
64
128
256
512
17
33
66
132
264
529
JAN
2012
APR
JUL
OCT
JAN
2013
APR
JUL
OCT
(b) wavelet real part spectrum
scale (day)
period (day)
JAN
2012
APR
JUL
OCT
JAN
2013
APR
JUL
OCT

Figure 6

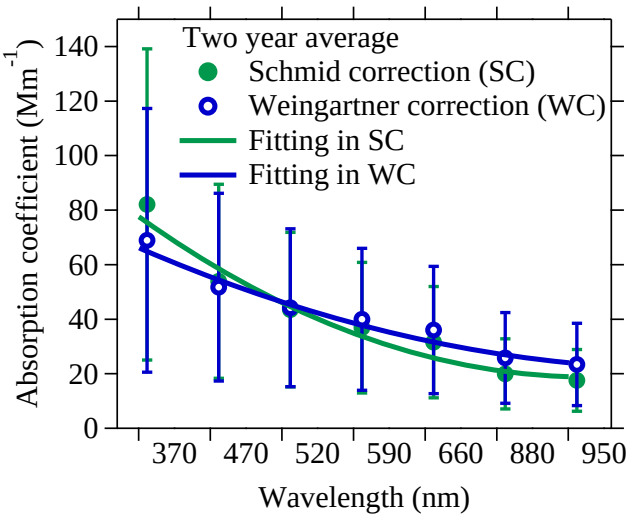

739

740 a)

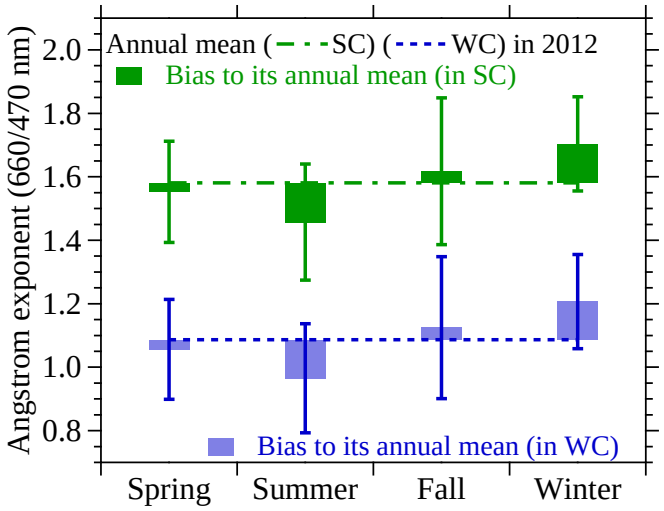

741

742 b)

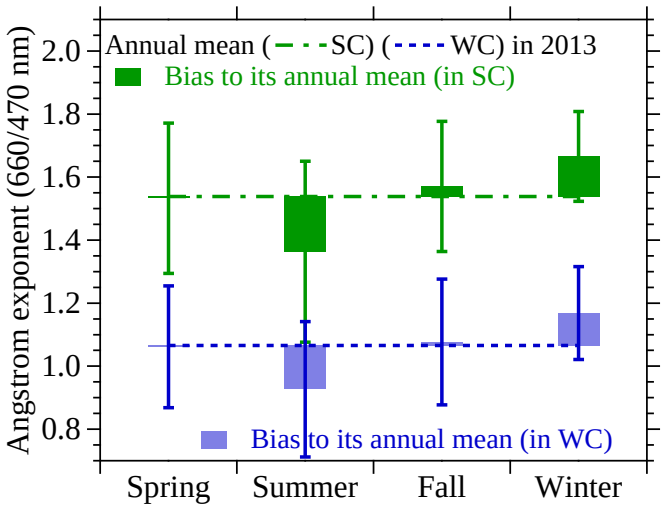

743

744 c)

745 Figure 7

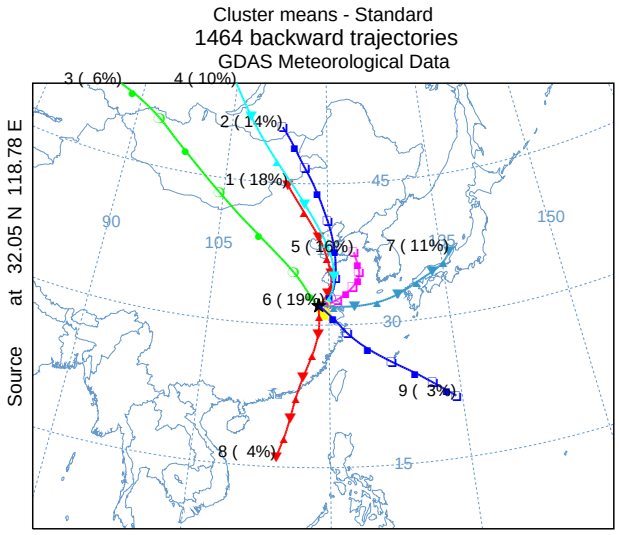

746

747 a)

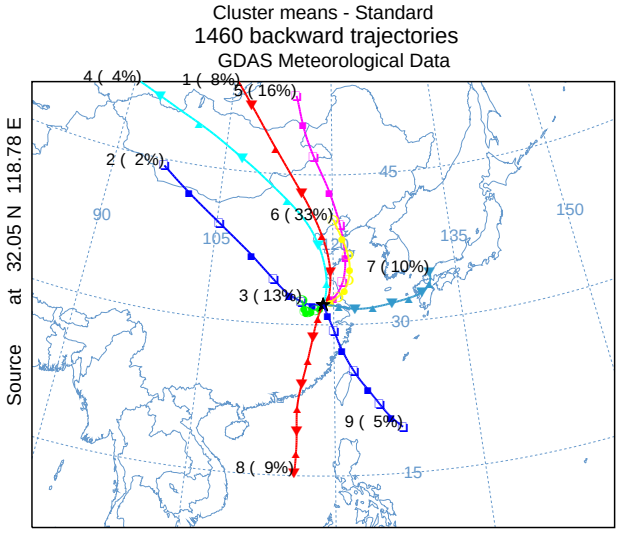

748

749 b)

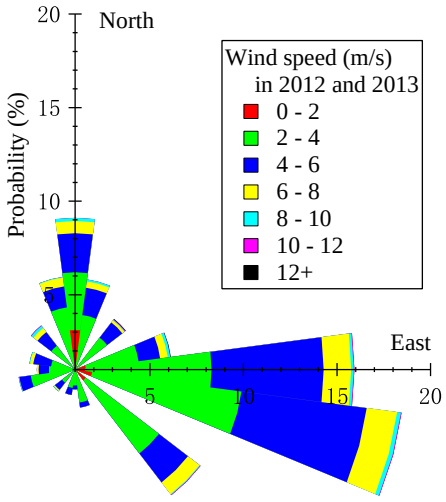

750

751 c)

752 Figure 8

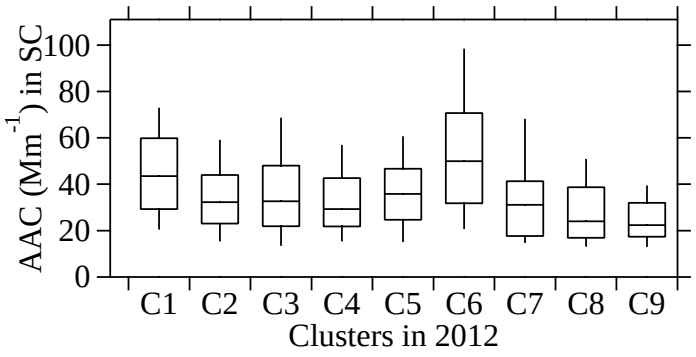

753

754 a)

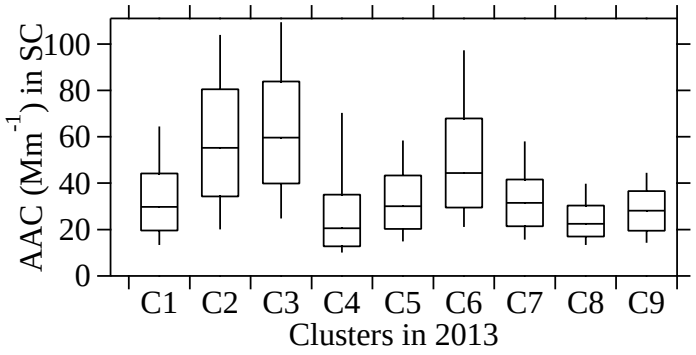

755

756 b)

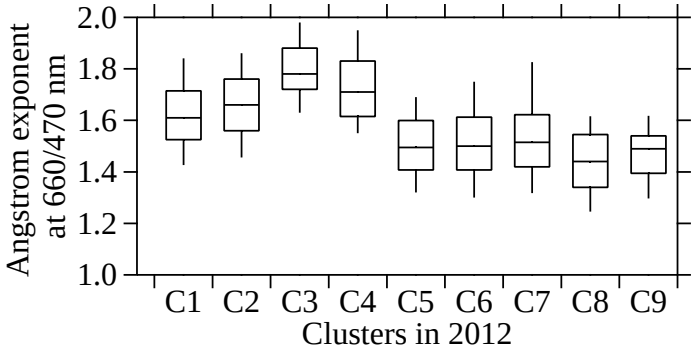

757

758 c)

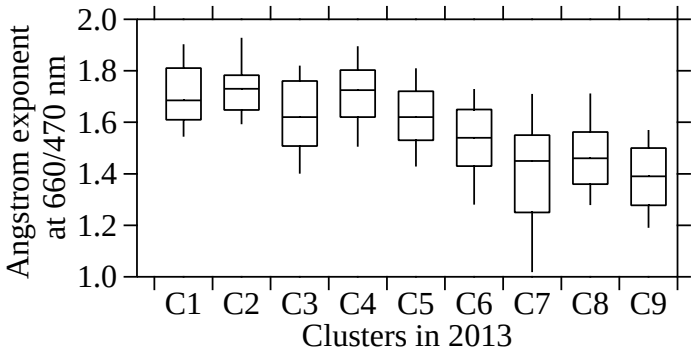

759

760 d)

761 Figure 9

762

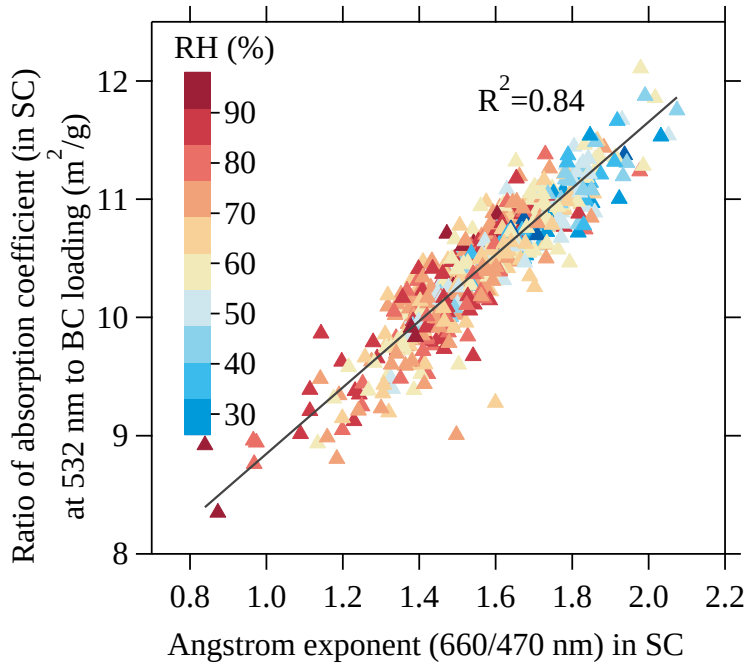

763

764 a)

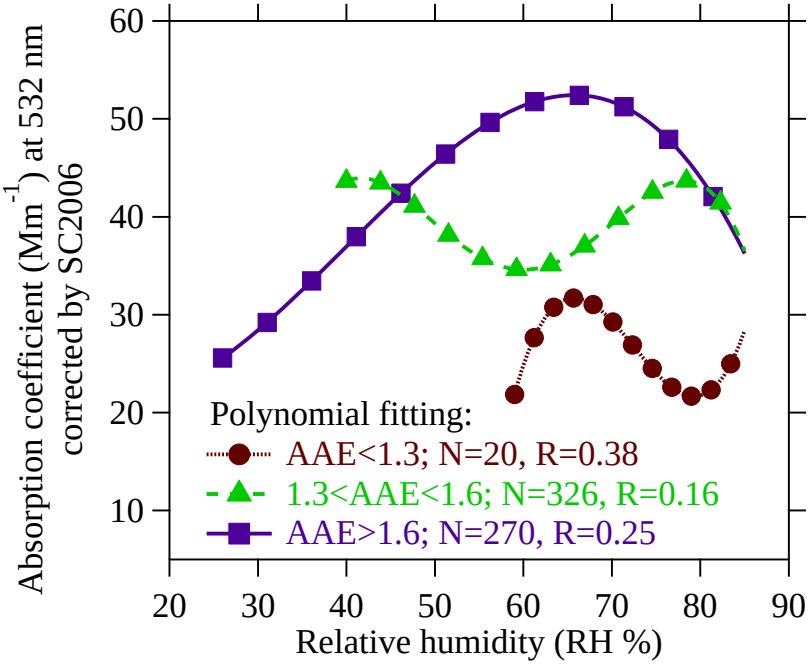

765

766 b)

767 Figure 10

768

769

770

771

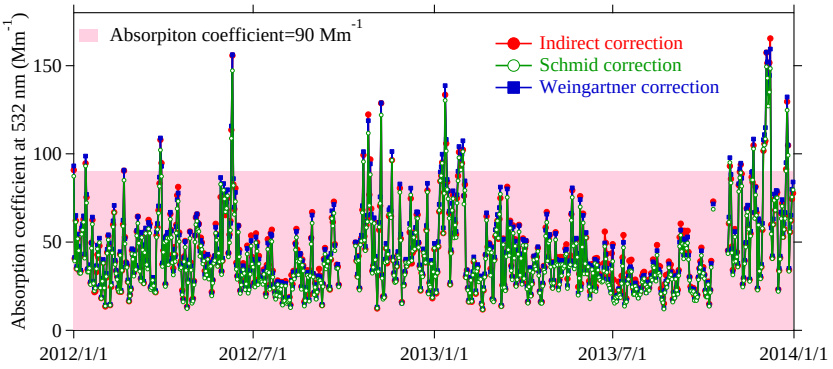

772

773 Figure 11

774

775